

5 SPATIAL DISTRIBUTION OF SCATTERERS IN THE CRUST OF GAURIBIDANUR SEISMIC ARRAY REGION (SOUTHERN INDIA)

5.1 INTRODUCTION

The three-dimensional spatial distribution of relative scattering coefficients in southern India is going to be estimated by means of an inversion technique applied to coda wave envelopes. The inversion technique implies mainly two steps. First we will follow the development outlined in Chapter 3. In this chapter we showed that to carry out the inversion it is necessary to solve a system of linear equations where the independent coefficients are the energy residuals computed from the seismograms, the unknowns correspond to the scattering coefficients in a certain small volume of the region under study, and the coefficients of each unknown indicate the importance of each small volume in the computation of a certain residual. This system of equations is huge and the number of unknowns and the number of equations is of the order of 10^5 .

There are several methods to invert such a system. Some of them are outlined in Chapter 4. For the first time in this kind of seismological research we will solve the system of equations by means of the Simultaneous Iterative Reconstruction Technique (SIRT) and Filtered Back-Projection method (FBP). Both algorithms are commonly used in biomedical applications but they have not been used previously to find spatial distribution of relative scattering coefficients.

SIRT algorithm has been previously described in section 4.3. SIRT allows to obtain more exact solutions than ART but it is slower. The Filtered Backprojection method was described in section 4.4 and its use to seismology was developed in section 4.5. It was shown to be much faster than any other non-iterative algorithm because each scattering coefficient can be simply computed as a weighted average of certain number of residuals. Filtered Backprojection has proved to provide very accurate reconstructions in biomedical applications and we will show that this is also valid in seismological applications.

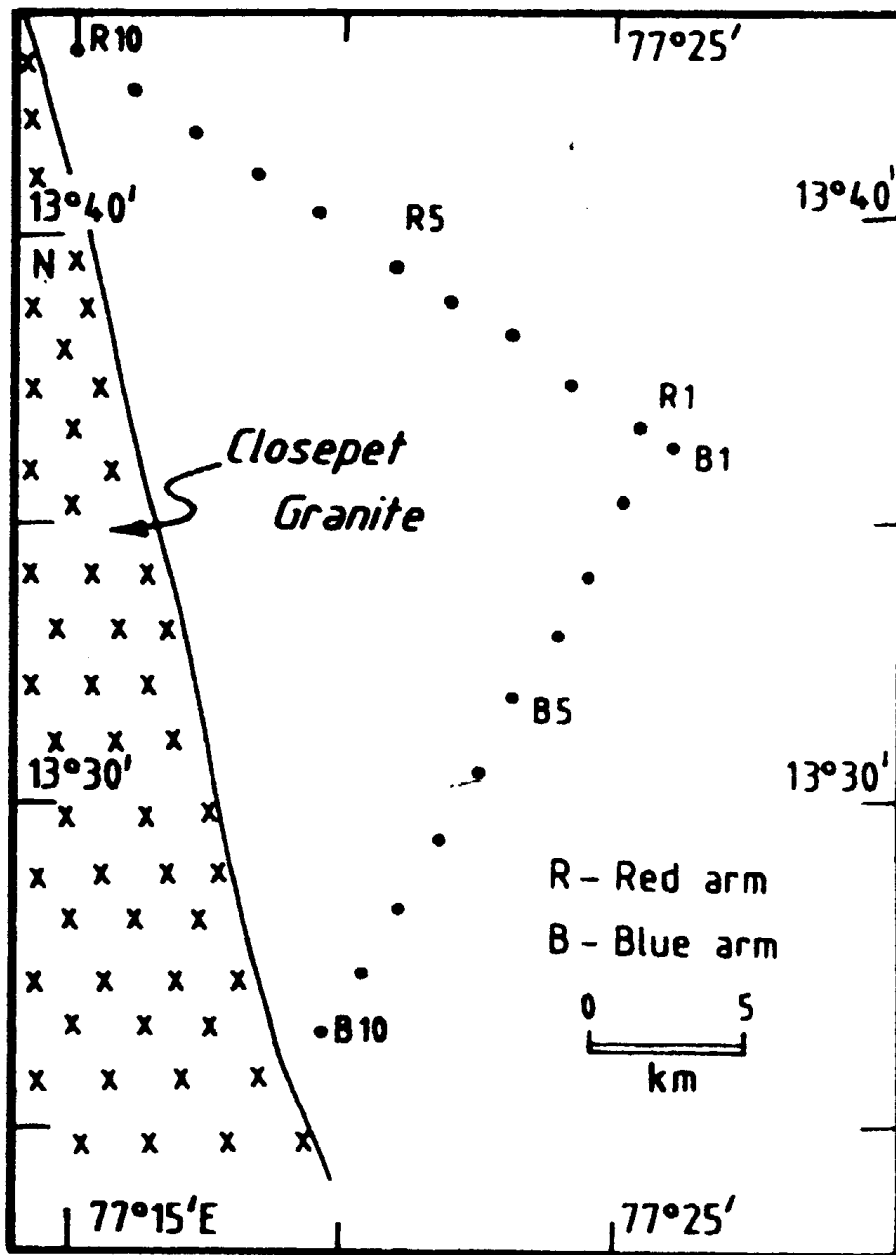


Figure 5-1. Geometry and location of stations of Gauribidanur seismic array [58].

5.2 GEOLOGICAL SETTING

The Gauribidanur seismic array is located in the Indian peninsula, about 90 km north of Bangalore, on the western flank of the eastern Dharwar craton which is one of the oldest geological provinces in southern India as sketched in Figure 5-2. The region, as can be

seen in Figure 5-3, is divided into the western (which is composed of old gneisses and greenstones with very few granites) and eastern (which is made of younger rocks with widespread N-S elongate plutons of late Archean granites) parts by the 400 km long and 20-30 km wide, north-south trending granitic intrusion named Closepet batholith (Moyen et al., 2003, [59]). We are going now to describe with a certain detail the main characteristics of the Dhawar Craton and the Closepet Batholith.

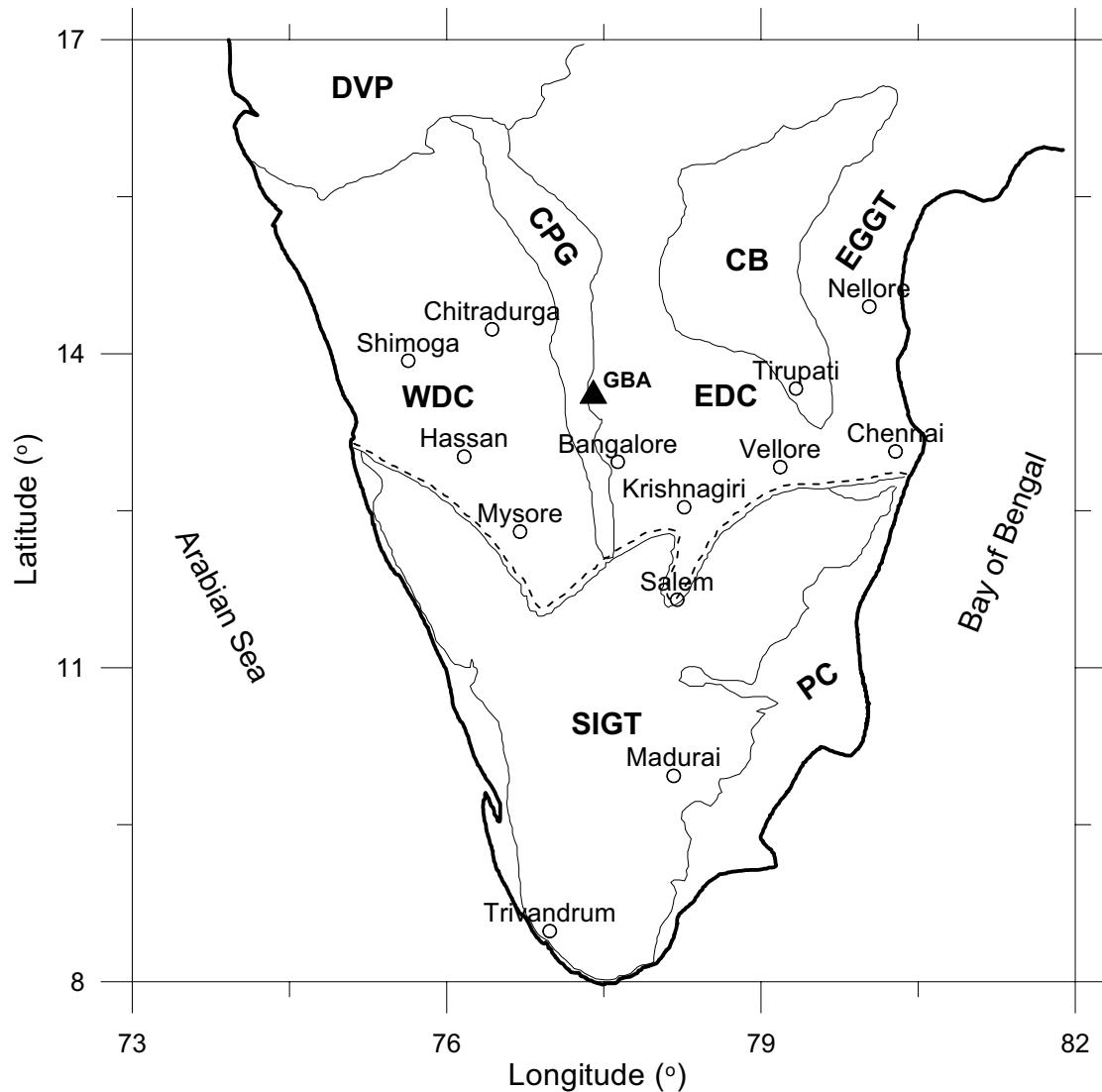


Figure 5-2. General geological sketch map of southern India. DVP, Deccan volcanic province; WDC, western Dharwar craton; EDC, eastern Dharwar craton; SIGT, south Indian granulite terrain; EGGT, eastern Ghat granulite terrain; CPG, closepet granite; CB, Cuddapah basin; PC, Phanerozoic sedimentary cover. Dotted line indicates Fermor's line (boundary between Dharwar craton and south India granulite terrain). (From Tripathi and Ugalde, 2004, [60]).

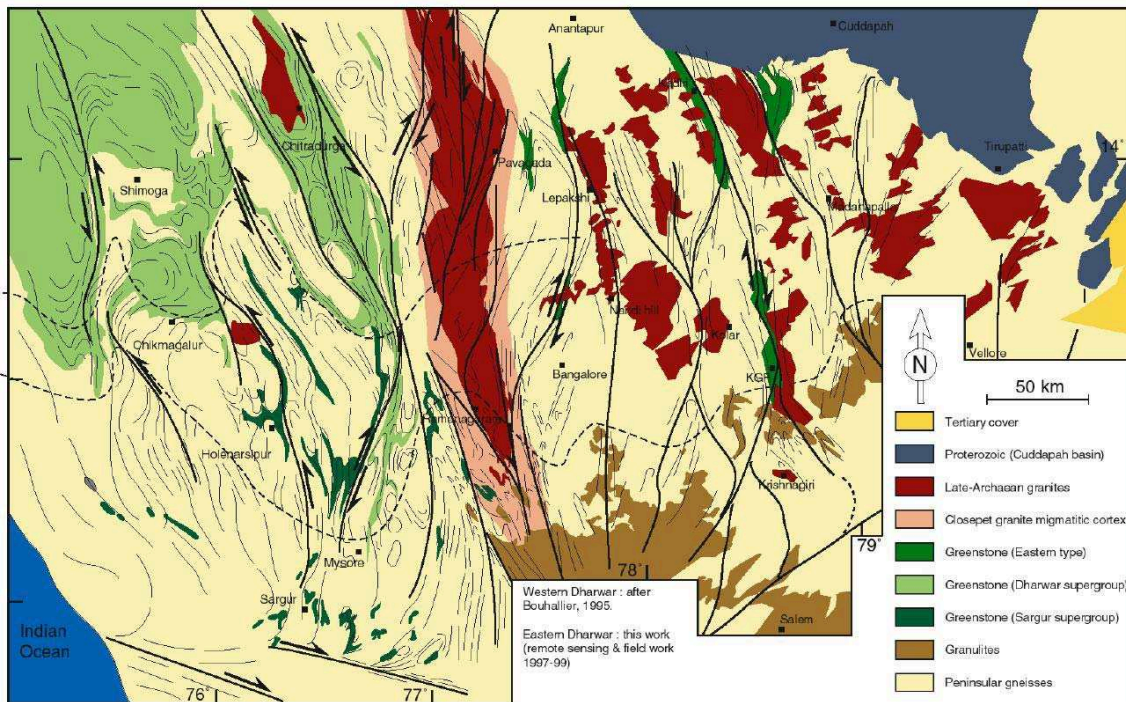


Figure 5-3. Detailed geological map corresponding to the eastern and western Dharwar craton and the Closepet granite batholith [61].

5.2.1 CLOSEPET GRANITE BATHOLIT

A batholith is a large emplacement of igneous intrusive (also called plutonic) rock that forms from cooled magma deep in the earth's crust. Igneous rocks are formed when magma cools and solidifies, with or without crystallization, either below the surface as intrusive (plutonic) rocks or on the surface as extrusive (volcanic) rocks. This magma can be derived from either the Earth's mantle or pre-existing rocks made molten by extreme temperature and pressure changes. The word "igneous" is derived from the Latin ignis, meaning "fire". Batholiths are almost always made mostly of felsic (silicate minerals or rocks) such as granite.

Although they may appear uniform, batholiths are in fact structures with complex histories and compositions. They are composed of multiple masses, or plutons, of magma that travelled toward the surface from a zone of partial melting at the base of the earth's crust. While moving, these plutons of relatively buoyant magma are called plutonic diapirs. Because the diapirs are liquefied and very hot, they tend to rise through the surrounding country rock, pushing it aside and partially melting it. Most diapirs do

not reach the surface to form volcanoes, but instead slow down, cool and usually solidify 5 to 30 kilometres underground as plutons (hence the use of the word pluton; in reference to the Roman god of the underworld Pluto).

A batholith is formed when many plutons converge together to form a huge expanse of granitic rock. Some batholiths are found paralleling past and present subduction zones and other heat sources for hundreds of kilometres in continental crust. An example of batholith, found predominantly in the mountains of western Canada, extends for 1,800 kilometres and reaches into south-eastern Alaska.

The word batholith is used by geographers to mean an exposed area of mostly continuous plutonic rock that covers an area larger than 100 square kilometres. However, the majority of batholiths visible at the surface (via outcroppings) have areas far greater than 100 square kilometres. These areas are exposed to the surface through the process of erosion accelerated by continental uplift acting over many tens of millions to hundreds of millions of years. This process has removed several tens of kilometres of overlying rock in many areas, exposing the once deeply buried batholiths.

Batholiths exposed at the surface are also subjected to huge pressure differences between their former homes deep in the earth and their new homes at or near the surface. As a result, their crystal structure expands slightly and over time. This manifests itself by a form of mass wasting called exfoliation. This form of erosion causes convex and relatively thin sheets of rock to slough off the exposed surfaces of batholiths (a process accelerated by frost wedging). The result is fairly clean and rounded rock faces.

The Closepet granite in southern India, is a large (400 km long but only 30km wide) elongate Late Archean granitic body. The Closepet granite was emplaced syntectonically within an active strike-slip shear zone. Structural levels from deep crust to upper levels crop out (see Figure 5-4). Despite local petrographic heterogeneities, a physical continuity of the porphyritic monzogranite can be observed all over the closepet structure. Consequently, the Closepet granite appears as a single magmatic body but different zones may be identified. Differential erosion has exposed it from the lower (25 km) to upper crust (5 km).

Four main parts are recognized from bottom to top (see Figure 5-4):

- i. The root zone is located south of 13°N. In the root zone, magmas were formed, collected and rose within active shear zones. The surrounding crust was highly ductile, leading to diffuse deformation. The root zone consists in a network of small dykes, plugs and sheets of granitoids injected in ductile shear zones and along foliation planes into Peninsular Gneisses. A wide range of magma compositions are found there, from monzonites (SiO₂= 51%) to granites (SiO₂= 75 %). It has been demonstrated that all magmatic facies result from magma mixing between a mafic, mantle-derived one, and a felsic one, generated by anatexis (partial melting of rocks, especially in the forming of metamorphic rocks) of the surrounding peninsular Gneisses.
- ii. A transfer zone, where the magma was progressively enriched in K-feldspar phenocrysts during its ascent. In this part, the granite rose as a mush moving as a whole within a less ductile crust. Slow cooling was responsible for a long magma residence time under conditions favouring to fabric enhancement and strain partitioning, leading to horizontal and vertical melt migration. There, a single, continuous mass (150 x 30 km) of porphyritic monzogranite (SiO₂= 65-70 %) intrudes the gneissic basement. The monzogranite results from magma mixing recognized in the root zone. In some narrow areas, corresponding to high strain zones on its margins, the Closepet granite is rich in enclaves of cumulate, mafic magmatic facies similar to those observed in the root zone. All these enclaves were carried upwards from deeper crustal levels. The same areas also commonly show K-feldspar phenocrysts accumulations.
- iii. A "gap" (dyke complex that acted as a filter zone), where the ascent of the mush was stopped, probably due to high phenocryst load and high viscosity contrast with the wall rocks. Only crystal-poor melts could continue their ascent through the dykes. The ascent of the mush is stopped at a level corresponding to the gap. At this level, only crystal-poor liquids are able to rise through a network of dykes, leaving below most crystals, and enclaves of all kinds.

- iv. A zone of shallow intrusions, where the liquids extracted from the mush filled small, elliptical plutons, cooling quickly and developing only very weak fabrics. The Closepet granite appears as a suite of small (commonly 10-30 km long), elliptical plutons crosscutting an gneissic basement. Individual intrusions display mutually cross-cutting relationships. In this area, only homogeneous, enclave-free granites ($\text{SiO}_2 = 70-75\%$) are found, at the exclusion of less differentiated facies. Porphyritic facies are rare, in marked contrast to the lower levels, where these facies are ubiquitous.

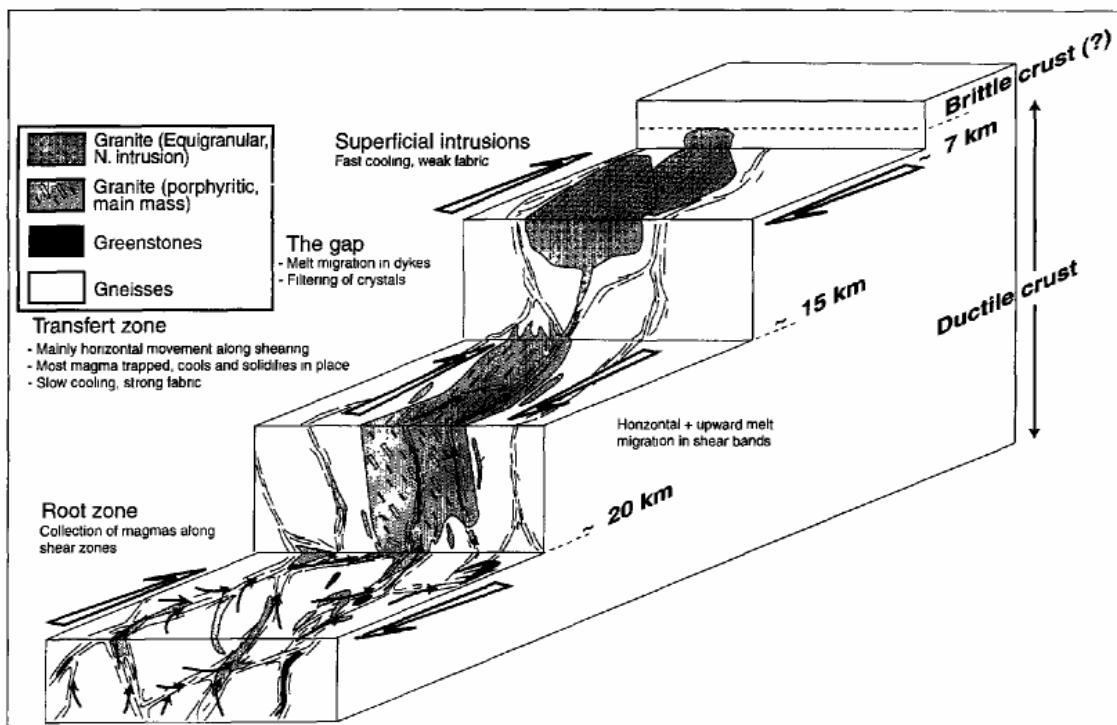


Figure 5-4. Sketch drawing of the emplacement mode and strain partitioning in the Closepet granite at contrasted structural levels (Moyen, 2000). Black, thin arrows correspond to melt movement. White, large arrows: kinematics of deformation. Notice three different zones may be defined along the batholith [59].

5.2.2 GENERAL CHARACTERISTICS OF CRATONS. THE DHAWAR CRATON

The continental crust is the layer of granitic, sedimentary and metamorphic rocks which form the continents and the areas of shallow seabed close to their shores, known as continental shelves. It is less dense than the material of the Earth's mantle and thus "floats" on top of it. Continental crust is also less dense than oceanic crust, though it

is considerably thicker; 20 to 80 km versus the average oceanic thickness of around 5-10 km. About 40% of the Earth's surface is now underlain by continental crust.

As a consequence of the density difference, when active margins of continental crust meet oceanic crust in subduction zones, the oceanic crust is typically subducted back into the mantle. Because of its relative low density, continental crust is only rarely subducted or re-cycled back into the mantle (for instance, where continental crustal blocks collide and overthicken, causing deep melting). For this reason the oldest rocks on Earth are within the cratons or cores of the continents, rather than in repeatedly recycled oceanic crust; the oldest continental rock is the Acasta Gneiss at 4.01 Ga, while the oldest oceanic crust is of Jurassic age.

A craton is then an old and stable part of the continental crust that has survived the merging and splitting of continents and supercontinents for at least 500 million years. Cratons are generally found in the interiors of continents and are formed of a crust of lightweight felsic igneous rock such as granite attached to a section of the upper mantle. A craton may extend to depth of 200 km.

Cratons are subdivided geographically into geologic provinces, each province being classified as an Archon, a Proton or a Tecton according to its age: Archons: consist of rocks from the Archean era, older than 2.5 billion years (2.5 Ga). Protons: consist of rocks from the early to middle Proterozoic era, older than 1.6 Ga. Tectons: consist of rocks from the late Proterozoic era, with ages between 1.6 Ga and 800 million years (800 Ma). The Dhawar Craton belongs to the Archean era (3.5-2.6 Ga).

As minerals (such as precious metals and diamonds) in the earth's crust tend to become separated with time, the oldest cratons are of the greatest interest to mining companies. This also applies to the Dhawar Craton; actually, mostly, our data comes from chemical explosions in mines).

The Dhawar craton is classically divided into three litological units:

- i. A gneissic basement of peninsular gneisses dated between 3.3 and 2.7 Ga. Gneiss is a common and widely distributed type of rock formed by high grade regional metamorphic processes from pre-existing formations that were originally either igneous or sedimentary rocks. Gneissic rocks are coarsely

foliated (typically by compositional banding due to segregation of mineral phases) and largely recrystallized. Gneisses that are metamorphosed igneous rocks or their equivalent are termed granite gneisses, granodiorite gneisses, etc. The word "gneiss" is from an old Saxon mining term that seems to have meant decayed, rotten, or possibly worthless material.

- ii. Greenstone belts overlying the gneisses, dated between 3.3 and 3.1 Ga for the oldest ones, and between 3.2 and 2.7 Ga for the younger ones. Greenstone is a non layered metamorphic rock derived from basalt or similar rocks containing sodium-rich plagioclase feldspar ($\text{NaAlSi}_3\text{O}_8$ (Albite)- $\text{CaAl}_2\text{Si}_2\text{O}_8$ (Anorthite)), chlorite ($(\text{Mg,Fe})_3(\text{Si,Al})_4\text{O}_{10}(\text{OH})_2 \cdot (\text{Mg,Fe})_3(\text{OH})_6$), epidote ($\text{Ca}_2(\text{Al,Fe})_3(\text{SiO}_4)_3(\text{OH})$) and quartz. Chlorite and epidote give the green colour.
- iii. Late Archean K-rich granitoids, consisting of N-S elongate bodies, among which the Closepet granite is the most spectacular. Several of these granites have been dated in the range 2.5 -2.6 Ga. Granite is a common and widely-occurring type of intrusive felsic igneous rock. Granites are usually a white or buff colour (a pale, light, or moderate yellowish pink to yellow) and are medium to coarse grained, occasionally with some individual crystals larger than the groundmass forming a rock known as porphyry. Granites can be pink to dark grey or even black, depending on their chemistry and mineralogy. Outcrops of granite tend to form tors (large hill, usually topped with rocks), rounded massifs, and terrains of rounded boulders (large rounded masses of rock lying on the surface of the ground or embedded in the soil) cropping out of flat, sandy soils.

The Dhawar craton is subdivided into western and eastern parts. The western Dhawar craton is made of 3.0-3.3 Ga old gneisses and greenstones, with very few 2.5 Ga granites; on the other hand, the eastern Dhawar Craton is made of younger (2.7-3.0 Ga) rocks with widespread elongate plutons of Late Archean granites. The Closepet granite represents the boundary between the two parts.

5.2.3 CHARACTERISTICS OF GAURIBIDANUR ARRAY'S SURROUNDING REGION

The area around the array is relatively flat (average elevation about 750 m), with a few hill ranges towards the east and the south. The rocks beneath the array are gneisses

and granites of Archean age. A thin layer of soil varying in thickness from 1.5 m to 4.5 m covers the siting area. Thus, the topographic influence on scattering would be very small. A crustal model consisting of a 16 km thick top granitic layer over a second layer 19 km thick above the mantle (i.e. with the Moho at 35 km depth) was proposed by Arora (1971) [62]. (Table 5-1).

5.3 DATA DESCRIPTION

Waveform data used consisted of selected 636 vertical-component, short period recordings of microearthquake codas from shallow earthquakes recorded by the Gauribidanur seismic array (GBA). They were selected from 80 earthquakes with epicentral distances up to 120 km which were recorded by the GBA in the period January 1992 to December, 1995. GBA is a seismic array that was sponsored by the U.K. Atomic Energy Authority (UKAEA) in the early sixties with the cooperation of the Bhabha Atomic Research Centre (BARC), Government of India. The array is L-shaped and each arm contains ten short-period ($T_0=1$ s) vertical-component Wilmore MkII seismometers spaced at intervals of about 2.5 km. The output of each instrument is carried by a telemetry system to a central laboratory where it is digitized at a sampling interval of 0.05 s and it is recorded in analog form on a 24-channel FM magnetic tape. All the events are shallow (depths less than 10 km) and local magnitudes range between 0.3 and 3.7 (see Figure 5.5).

5.4 DATA ANALYSIS

Each seismogram was bandpass-filtered over the frequency bands 1-2 (1.5 ± 0.5) Hz, 2-4 (3 ± 1) Hz and 4-10 (7 ± 3) Hz. Then, the rms amplitudes $A_{\text{obs}}(f|r,t)$ were calculated by using a 0.25 s spaced moving time window of length $t\pm 2$ s, $t\pm 1$ s, and $t\pm 0.5$ s for the first, second and third frequency band, respectively. The time interval for the analysis started at 1.5 times the S-wave travel times (in order to increase the resolution near the source region) and had a maximum length of 20 s (to minimize the effects of multiple scattering). The rms amplitudes for a noise window of 10 s before the P-wave arrival were also computed and only the amplitudes greater than two times

the signal to noise ratio were kept. The amplitudes were then corrected for geometrical spreading by multiplying by t^2 which is valid for body waves in a uniform medium. Then, the average decay curve was estimated for each seismogram by means of a least-squares regression of $\ln[t^2 A_{\text{obs}}(f|r,t)]$ vs. t and only the estimates with a correlation coefficient greater than 0.60 were kept. The observed coda residuals $e(t)$ were then calculated by taking the ratio of the corrected observed amplitudes to the estimated exponential decay curve. Finally the residuals were averaged in time windows of $\delta t = 0.5$ s to get e_j at discrete lapse times t_j . The decrease of δt increases the spatial resolution, but also the size of the inversion problem.

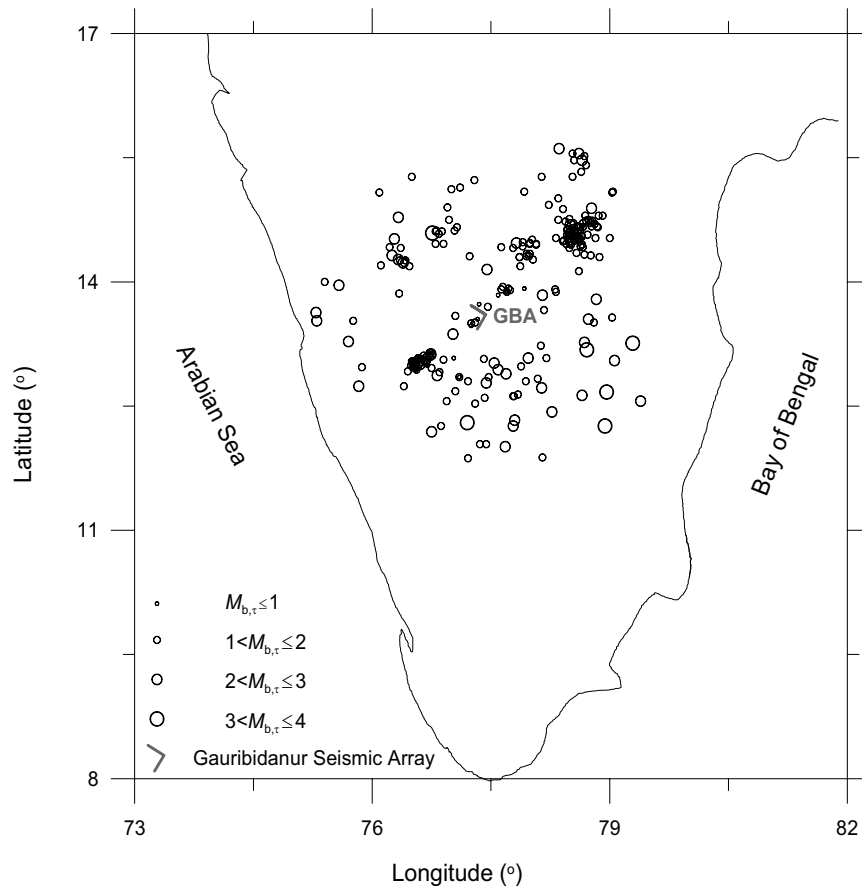


Figure 5-5. Map of southern India showing the location of the seismic stations and earthquakes used for the analysis [60].

The time window for the averaging must also satisfy the condition $\delta t \leq 2(\delta V)^{1/3} / \beta$, where δV is the volume of one small block into which the study area is divided and $\beta=3.65 \text{ km}\cdot\text{s}^{-1}$ in this region (Arora, 1971, [62]; Krishna & Ramesh, 2000, [63]). This condition assures that the width of each spheroidal shell is smaller than the size of a block. All this process is illustrated in Figure 5-6 where we show the following: Figure (a) corresponds to a band-pass filtered coda waveform of an earthquake at an epicentral distance of 90.6 km in a region around Gauribidanur array (India). Figure (b) corresponds to the logarithm of the running mean-squared amplitudes corrected for geometrical spreading effect. The discontinuous line is the best linear fitting function to the logarithmic trace. Finally, figure (c) corresponds to the logarithm of the coda energy residuals averaged in a time window of 0.5 s.

The corresponding system of equations to solve is (see Chapter 3):

$$\begin{aligned}
 w_{11}\alpha_1 + \dots + w_{i1}\alpha_i + \dots + w_{N1}\alpha_N &= e_1 \\
 &\vdots \\
 w_{1j}\alpha_1 + \dots + w_{ij}\alpha_i + \dots + w_{Nj}\alpha_N &= e_j \\
 &\vdots \\
 w_{1M}\alpha_1 + \dots + w_{iM}\alpha_i + \dots + w_{NM}\alpha_N &= e_M
 \end{aligned} \tag{5.1}$$

In this case, the system has a number of equations $M \simeq 2700$ for the frequency bands centred at 1.5 Hz and 7 Hz, and $M \simeq 5200$ equations for the 3 Hz centre frequency. To write the system, we considered a 155 km x 155 km in horizontal and 80 km in depth study region attending to the stations and hypocenters distribution and it was divided into $N=50 \times 50 \times 25$ blocks. This means we have $N=62500$ unknowns in Eq. (5.1). To write the system, it is important also to know the velocity of S waves. Then, the observational system of equations (Eq. (5.1)) was created by assuming the layered velocity structure by Arora (1971, [62]) (see table Table 5-1) and it was solved using the SIRT and FBP algorithms (see Chapter 4).

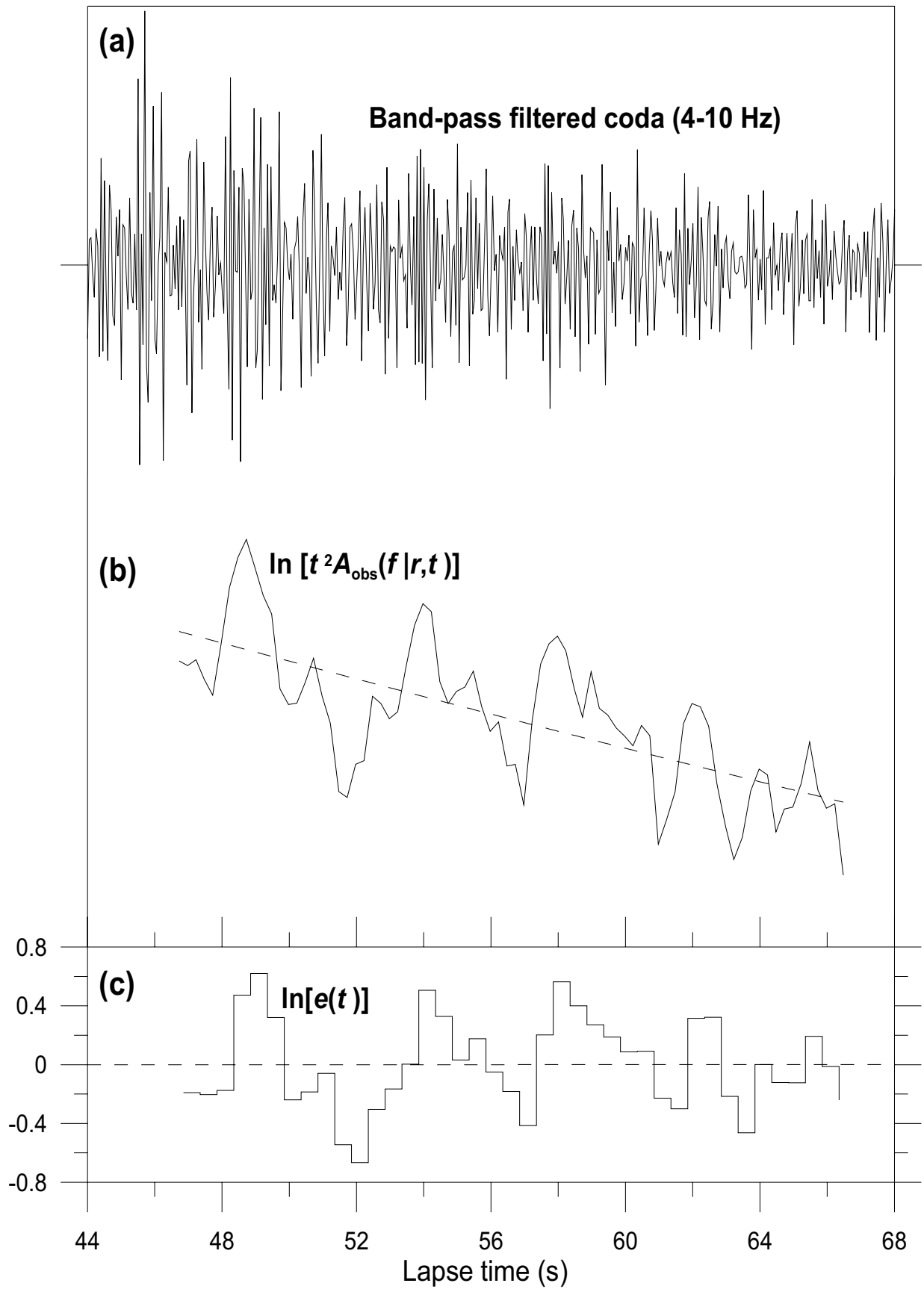


Figure 5-6 Illustrating the process to calculate the coda energy residuals for a GBA seismic event

| Depth (km) | S-wave velocity (km/s) |
|-------------------|------------------------|
| $0 < z < 15.8$ | 3.46 |
| $15.8 < z < 34.7$ | 3.96 |
| $z > 34.7$ | 4.61 |

Table 5-1. S-wave velocity model for the Gauribidanur region.

5.5 RESULTS

Before discussing the results, we will examine the reliability of the solution. Figure 5-7 plots the hit counts, or number of coda residuals contributed by each block, that shows which grid zones may be affected by sampling insufficiency for the grid defined. It can be observed that the entire region is sampled by the ellipses, however, the hit counts are much less in an area close around the array and they increase both in horizontal and depth directions up to the considered depth of 80 km. This happens because the stations are concentrated in a small area, which makes all the blocks which are close to the array to correspond to short lapse times, and they are few because we omitted the earliest portion of the S-wave coda by adopting $1.5t_s$ as start time for the analysis.

On the other hand, we tested the resolution of the inversion methods by synthesizing the coda energy residuals from the observational equation using a given test distribution of scattering coefficients and the same distribution of stations and events used in the analysis. We generated vertical structures with positive perturbations of the scattering coefficient with horizontal dimensions equal to one block and depths up to 80 km embedded in a non perturbed medium.

Then the synthesized residuals were inverted. Results show that although the vertical structures are seen almost up to the maximum depth considered of 80 km, they are well reproduced (more than 50% of the perturbation value is returned) only up to the seventh block (22.4 km). The results are shown in Figure 5-8.

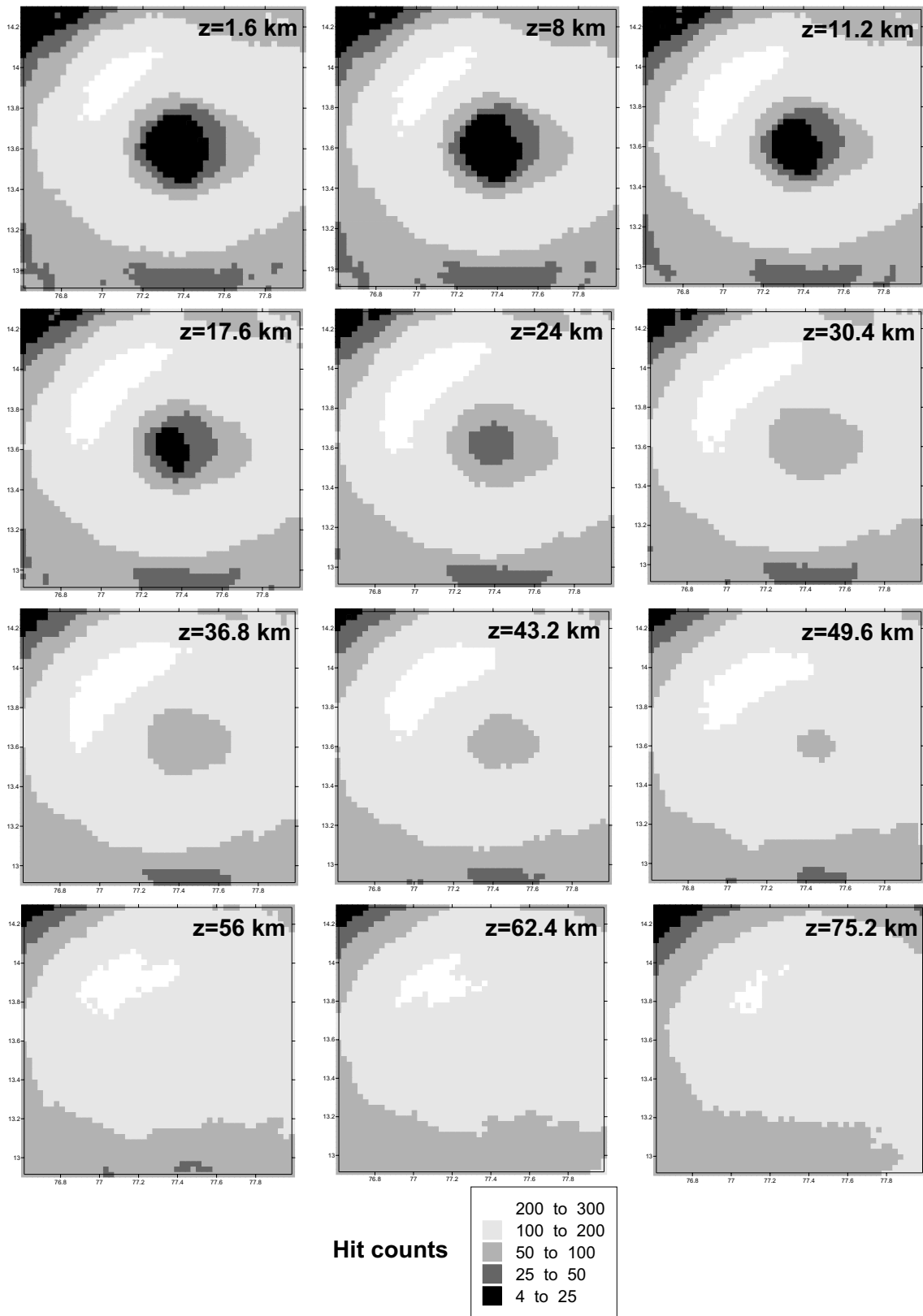


Figure 5-7. Hit counts or number of coda residuals contributed by each block. It measures the number of times each block is sampled by the scattering shells of observed coda data. The darker areas are the zones lesser sampled by the spherical shells.

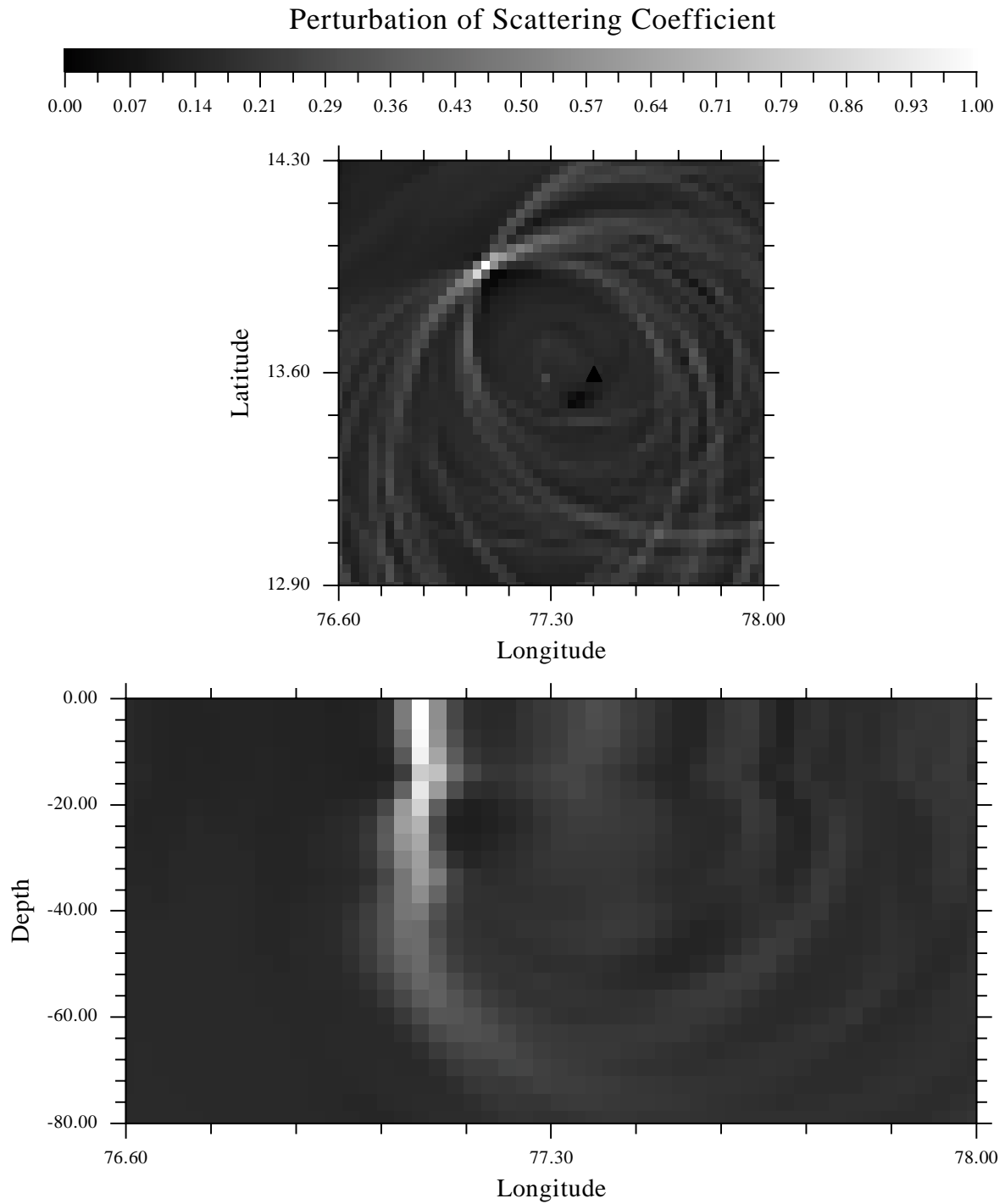


Figure 5-8. Spatial distribution of relative scattering coefficients for a synthetic test consisting of a column. It was located northeast from the array centre point, which is shown by a solid triangle. A longitudinal section corresponding to $z=0$ km and the corresponding transversal section are shown.

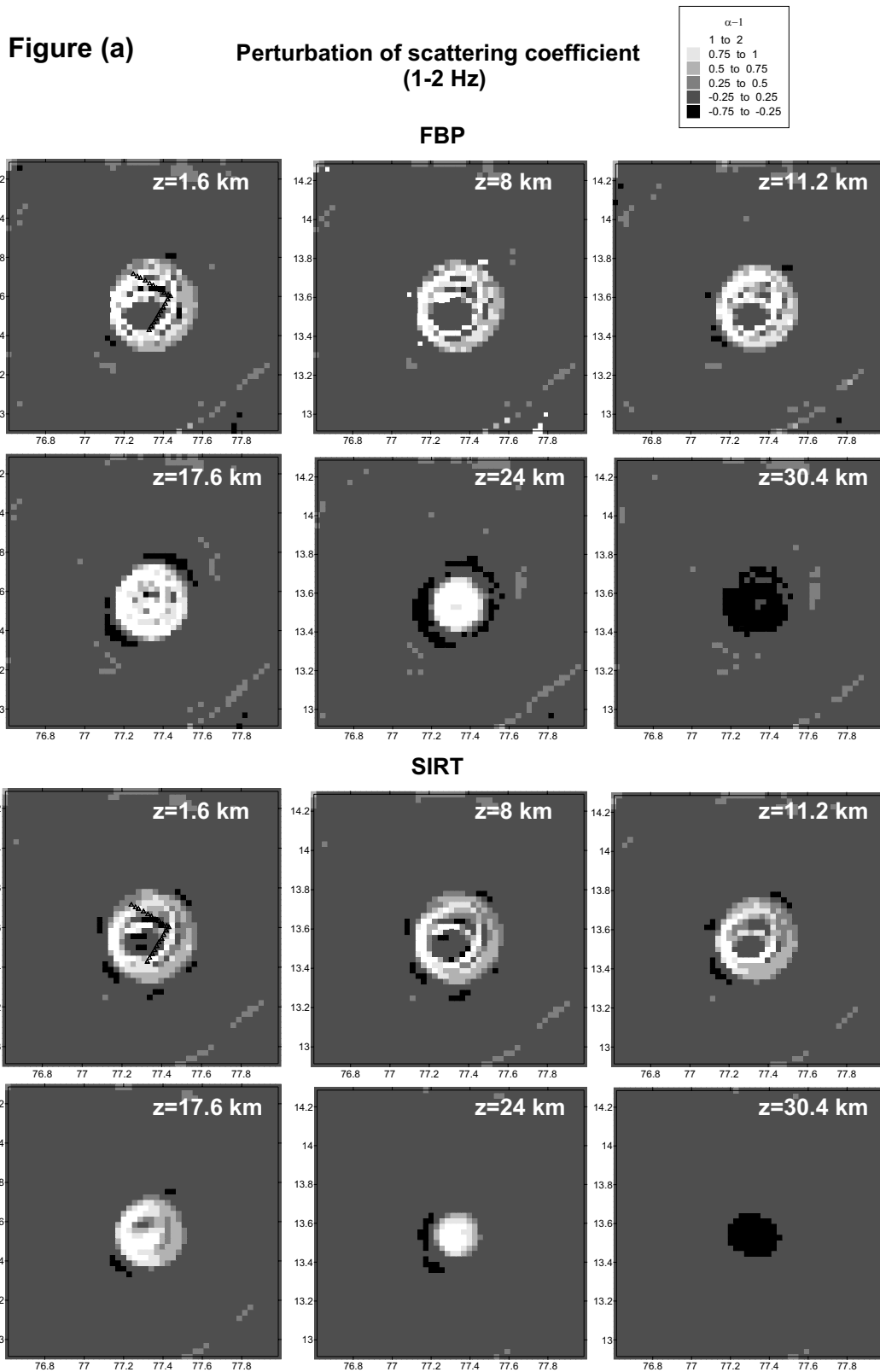
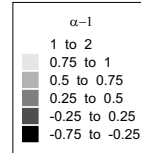


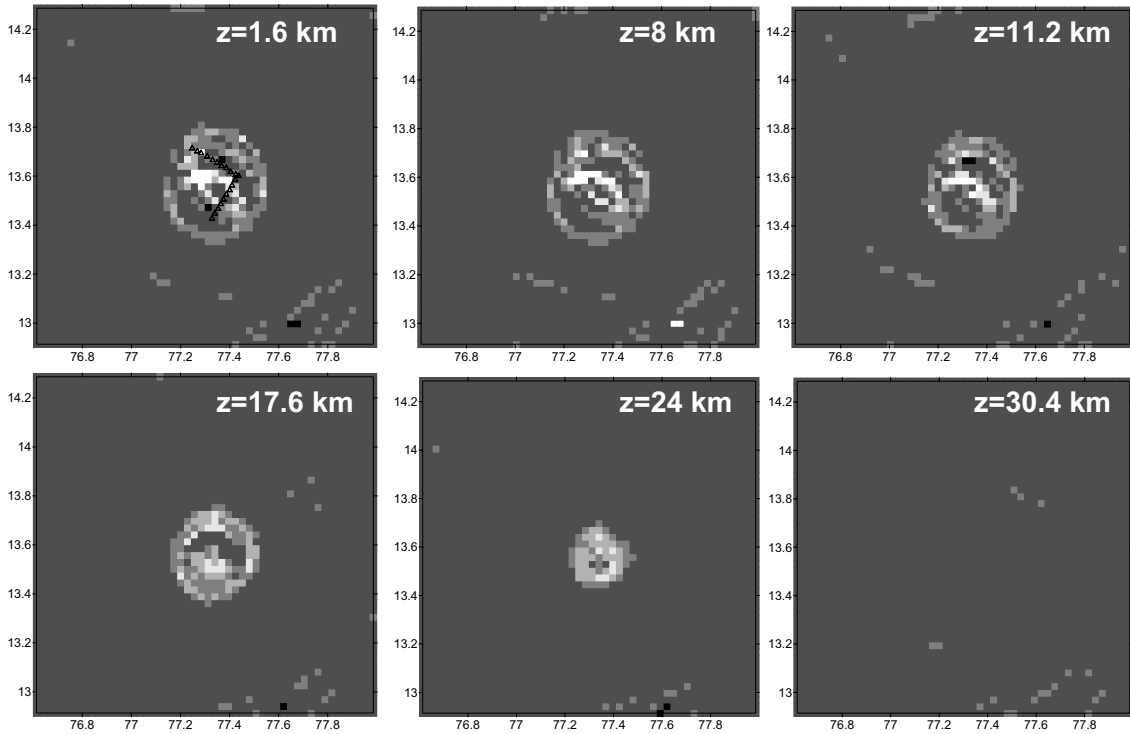
Figure 5-9. Spatial distribution of relative scattering coefficients for different depths and for the two inversion methods used: (a) results for the frequency band 1-2 Hz; (b) 2-4 Hz; and (c) 4-10 Hz. The lightest zones indicate the strongest perturbations from an average scattering coefficient.

Figure (b)

Perturbation of scattering coefficient
(2-4 Hz)



FBP



SIRT

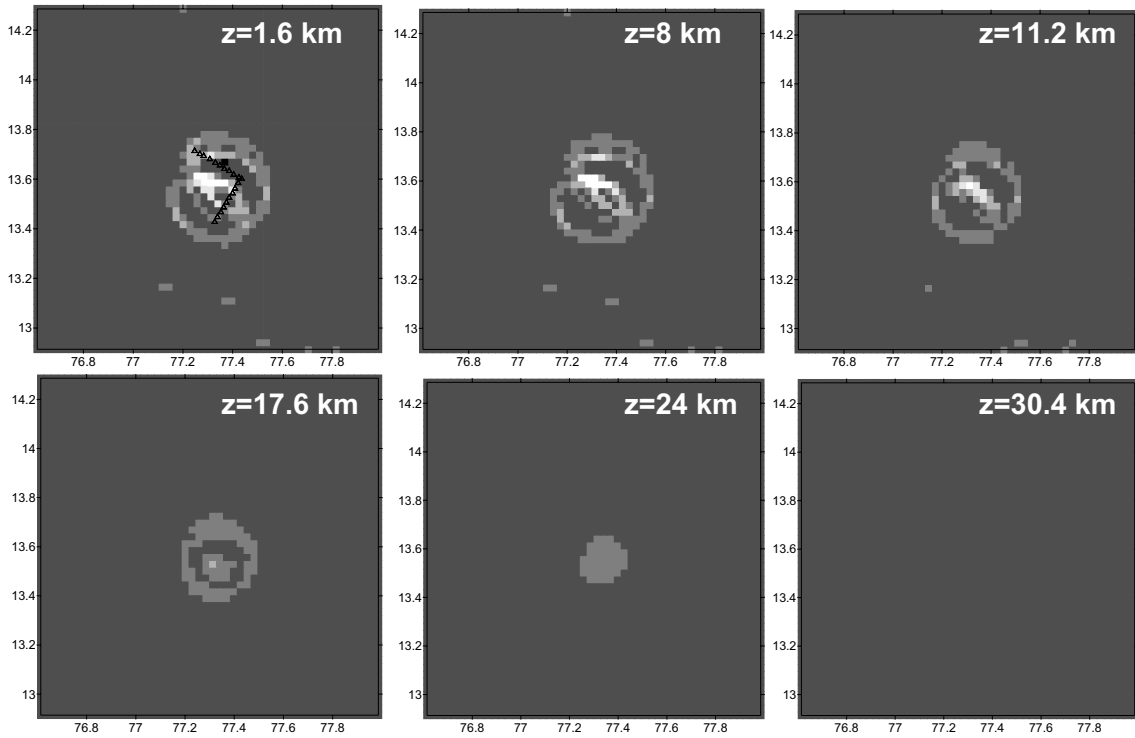
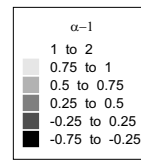


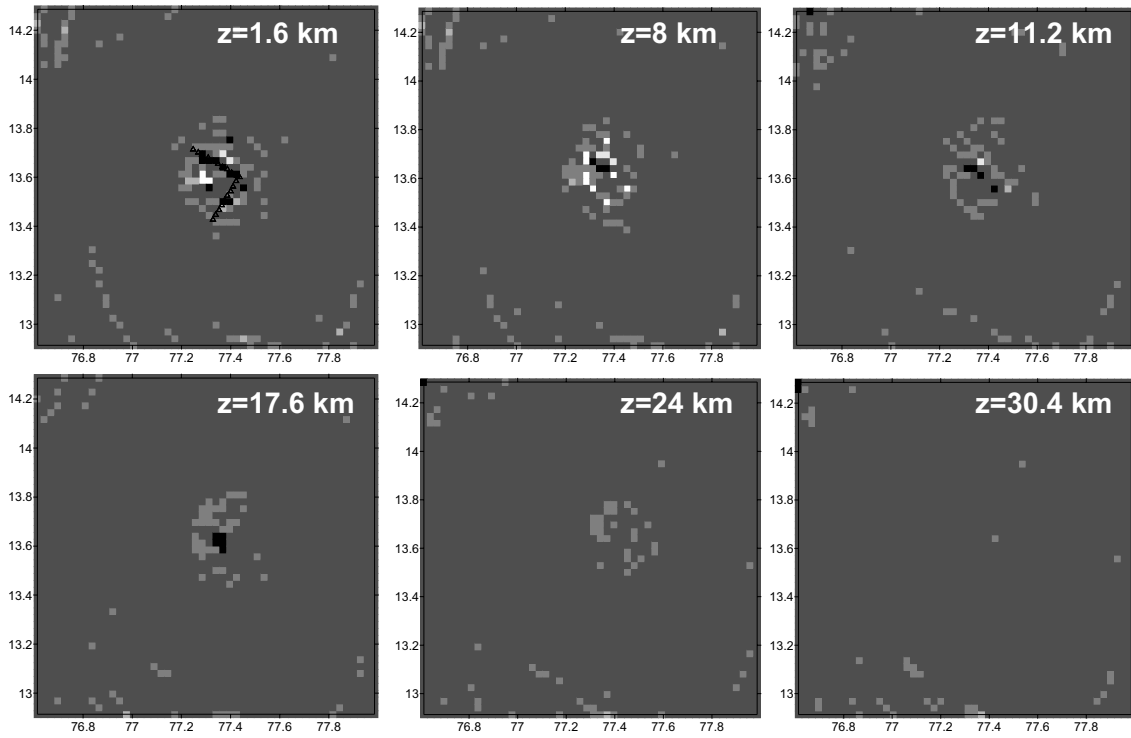
Figure 5-9. (continued)

Figure (c)

Perturbation of scattering coefficient
(4-10 Hz)



FBP



SIRT

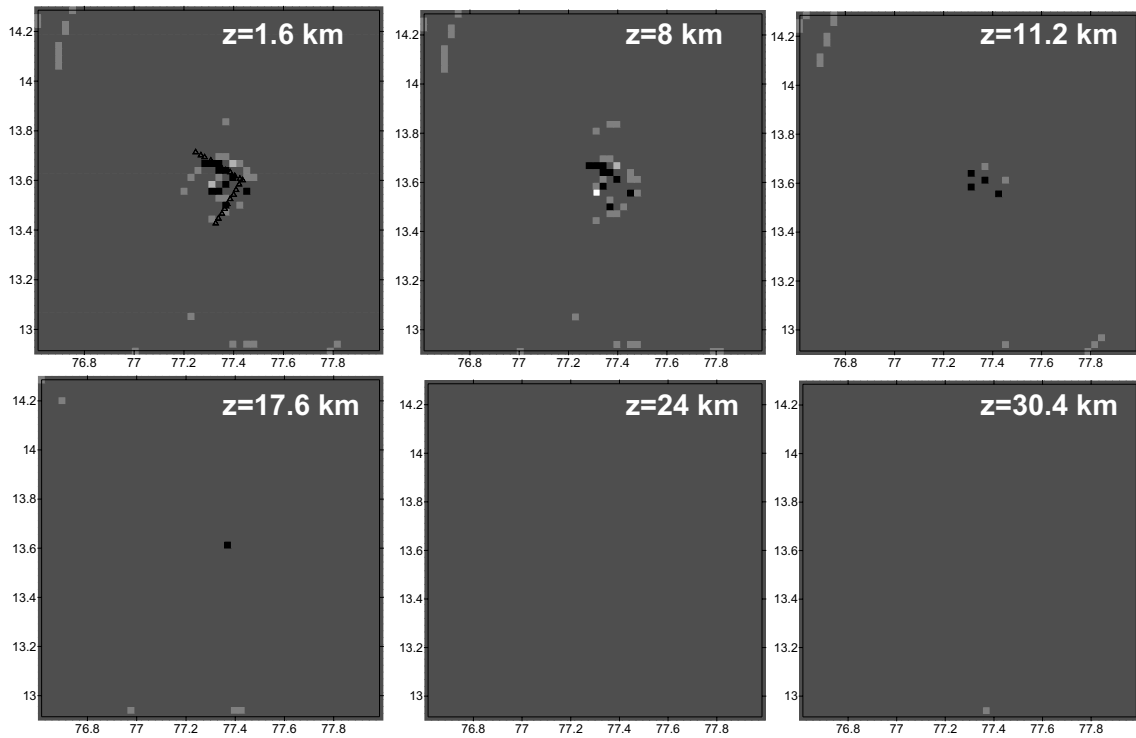


Figure 5-9. (continued)

The resulting distribution of relative scattering coefficients $\alpha - 1 = \frac{g - g_0}{g_0}$ in the study region for the three analyzed frequency bands and for different depths is plotted in Figure 5-9. The lightest tones indicate scattering coefficients larger than the average in this region.

5.6 DISCUSSION

It can be observed that we obtain practically the same distribution of relative scattering coefficients regardless of applying the SIRT or FBP inversion algorithms. Whereas the SIRT algorithm provides slightly lower values of the relative scattering coefficients, the FBP method provides more contrast. Thus, we would recommend the use of the FBP method, which requires much lesser (about 100 times) computation time.

On the other hand, Figure 5-9 shows that more than the 90% of the analyzed region reveals a spatial perturbation of the scattering coefficient between $\pm 25\%$. This means that the crust around GBA presents a remarkably uniform distribution of scattering coefficients. For low frequencies, this uniformity is broken by the presence of a strong scattering area which is recognized from the surface up to a depth of 24 km just below the array. This structure is not observed at high frequencies. In fact, each analyzed frequency band is giving us information about inhomogeneous structures with sizes comparable to the seismic wavelengths (~ 1.8 to ~ 3.6 km for 1-2 Hz, ~ 900 m to ~ 1.8 km for 2-4 Hz, and ~ 360 m to ~ 900 m for 4-10 Hz in this case). Figure 5-10 shows a cross section of relative scattering coefficients shown in Figure 5-9 projected onto the vertical plane defined by the parallel of the array centre point. It can be observed that the strongest scatterers are located on the western part of GBA. However, Figure 5-9 and Figure 5-10 show that the heterogeneity follows an ellipsoidal pattern. This may happen because this area is poorly sampled by the ellipses as previously discussed in Figure 5-7, however, the behaviour is only observed for the lowest frequency band analyzed. In fact, we detected high values of the residuals at low frequencies and short lapse times. In order to establish the validity of the results of this study we tested the inversion method by means of a synthetic test.

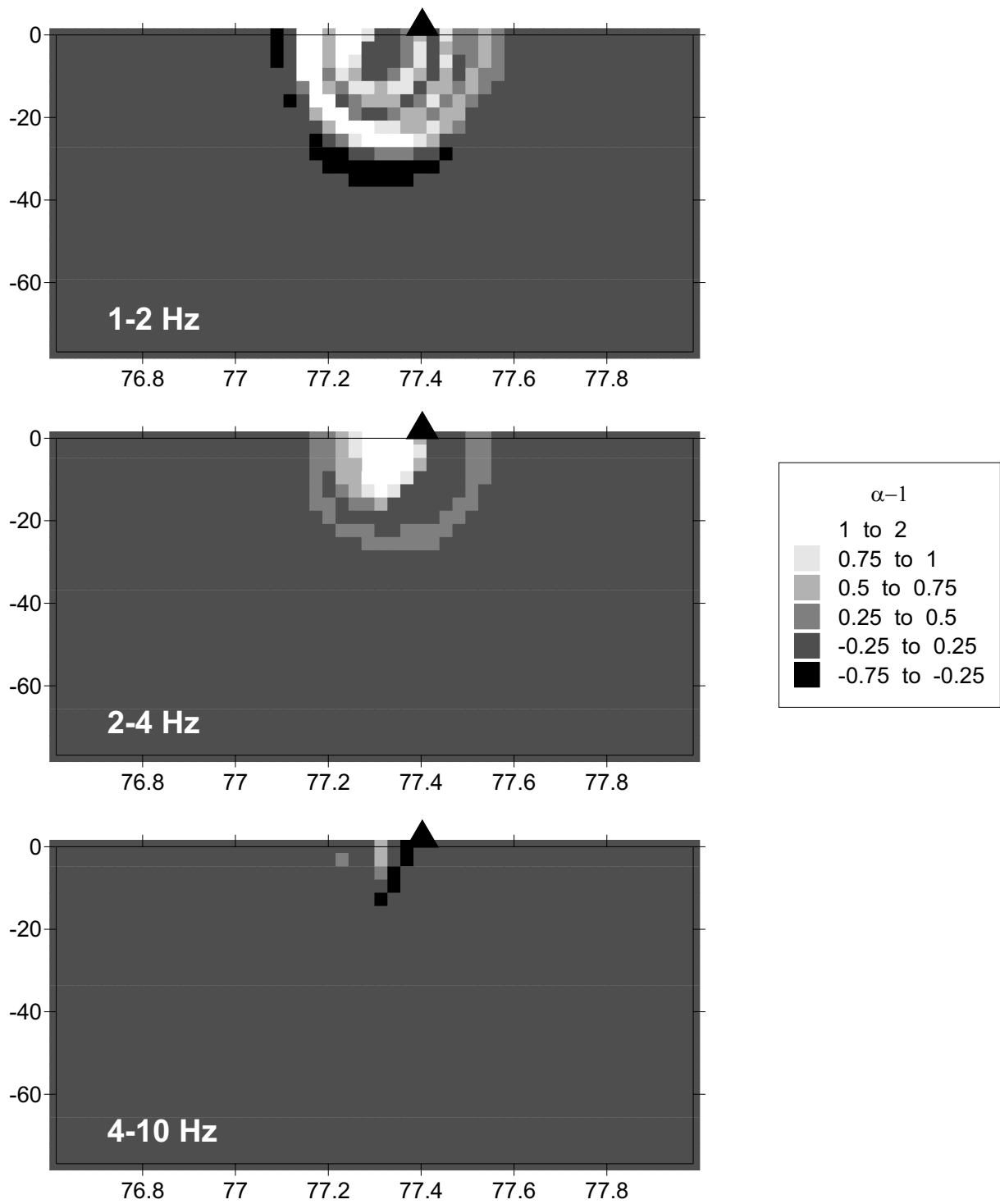


Figure 5-10. Vertical cross section of relative scattering coefficients at the parallel 13.6°, which corresponds to the latitude of the array cross-point.

Because the most notable geological feature in the considered region is the 400 km long and 20-30 km wide, north-south trending Closepet granitic intrusion, we simulated the existence of a single spheroidal structure with positive perturbations of the scattering coefficient at different locations in a non-perturbed medium.

Results of the inversion of the synthesized residuals are shown in Figure 5-11. It can be observed that the patterns of the test are well reproduced. We may then conclude that the scattering region observed near the array centre point (Figure 5-9) is neither a ghost image nor a mathematical artefact. Thus we may consider that the inversion method may reproduce up to a certain extent the observed data.

With respect to the uniform distribution of scattering coefficients, our results are in accordance with previous studies performed in the region. In an early work in this region using statistical analysis of observed teleseismic traveltime residuals, Berteussen et al. (1977) [64] remarked that the area on which GBA is sited presents exceptionally homogeneous structures, apart from the general existing velocity perturbations of the order of a few percent. This conclusion was partly supported by Mohan & Rai (1992) [58], who also detected the presence of a prominent scatterer in the deep crustal and uppermost mantle level (30-55 km) in this region from a semblance technique analysis. The scattering region coincided with the Closepet granitic intrusion in the region. Krishna & Ramesh (2000) [63] performed a frequency-wavenumber ($f-k$) spectral analysis of P-coda waveforms to mine tremors and explosions recorded at GBA array. They found a near-on azimuth dominant energy peak with apparent velocity appropriate to the upper crustal depths and they interpreted the result by the presence of a scattering waveguide at upper crustal depths (5-15 km) which might be also related to the granitic batholith. In our case, the zone of strong relative scattering coefficients at low frequency to the west of the GBA array cross-point also coincides with the so-called Closepet batholith, which is a granitic intrusion that acts as the major geological boundary in the region and it is believed to be a Precambrian suture zone between the eastern and western Dharwar craton.

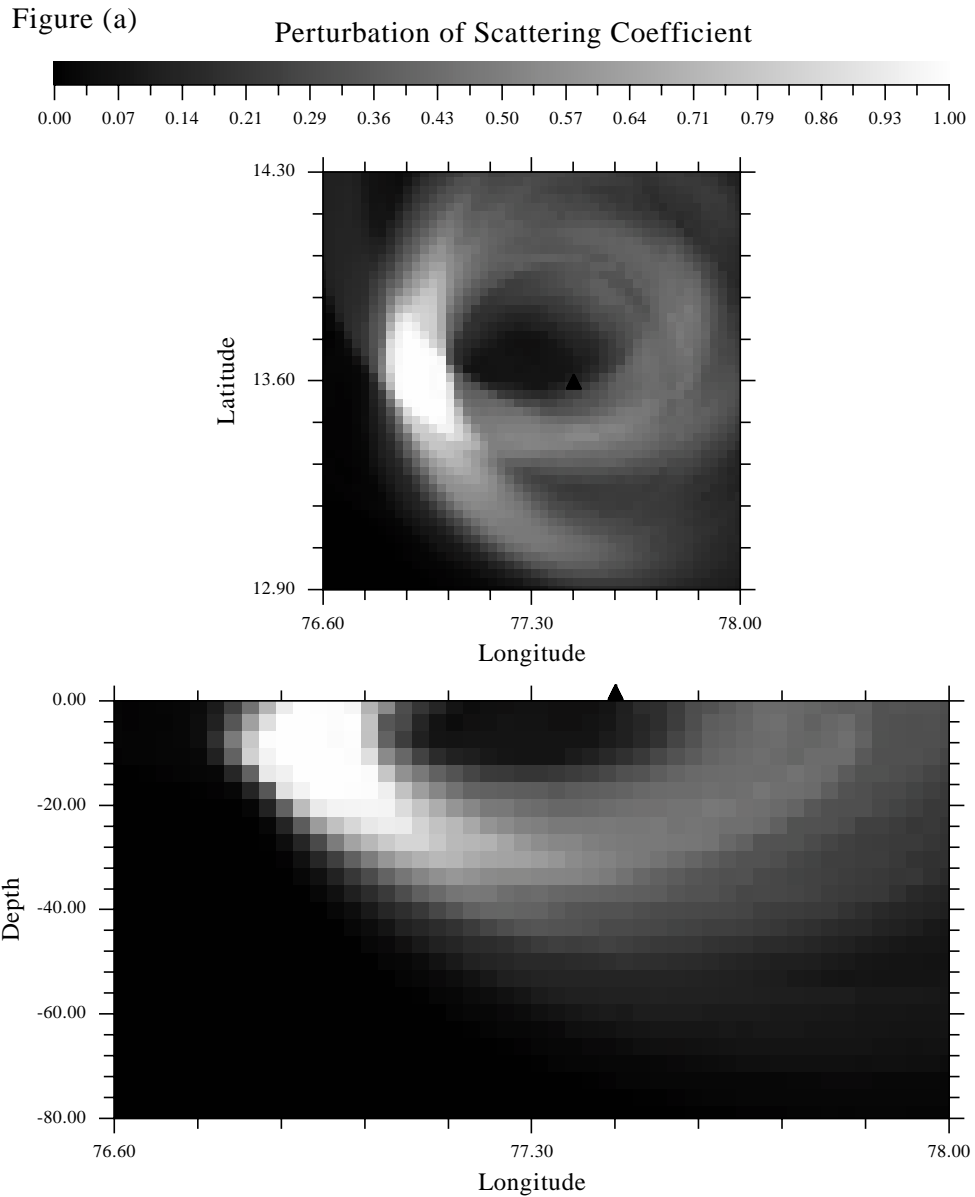


Figure 5-11. Spatial distribution of relative scattering coefficients for a synthetic test consisting of one spheroidal structure with two horizontal semi-axes of 13 km and the vertical semi-axis of 9.3 km. It was located at different distances from the array centre point, which is shown by a solid triangle: (a) to the west; (b) below; and (c) to the east. The pattern recovered at a depth of 0 km is plotted at the top of the figure. The vertical cross section along the plane defined by the latitude of the array centre point is also shown.

Figure (b)

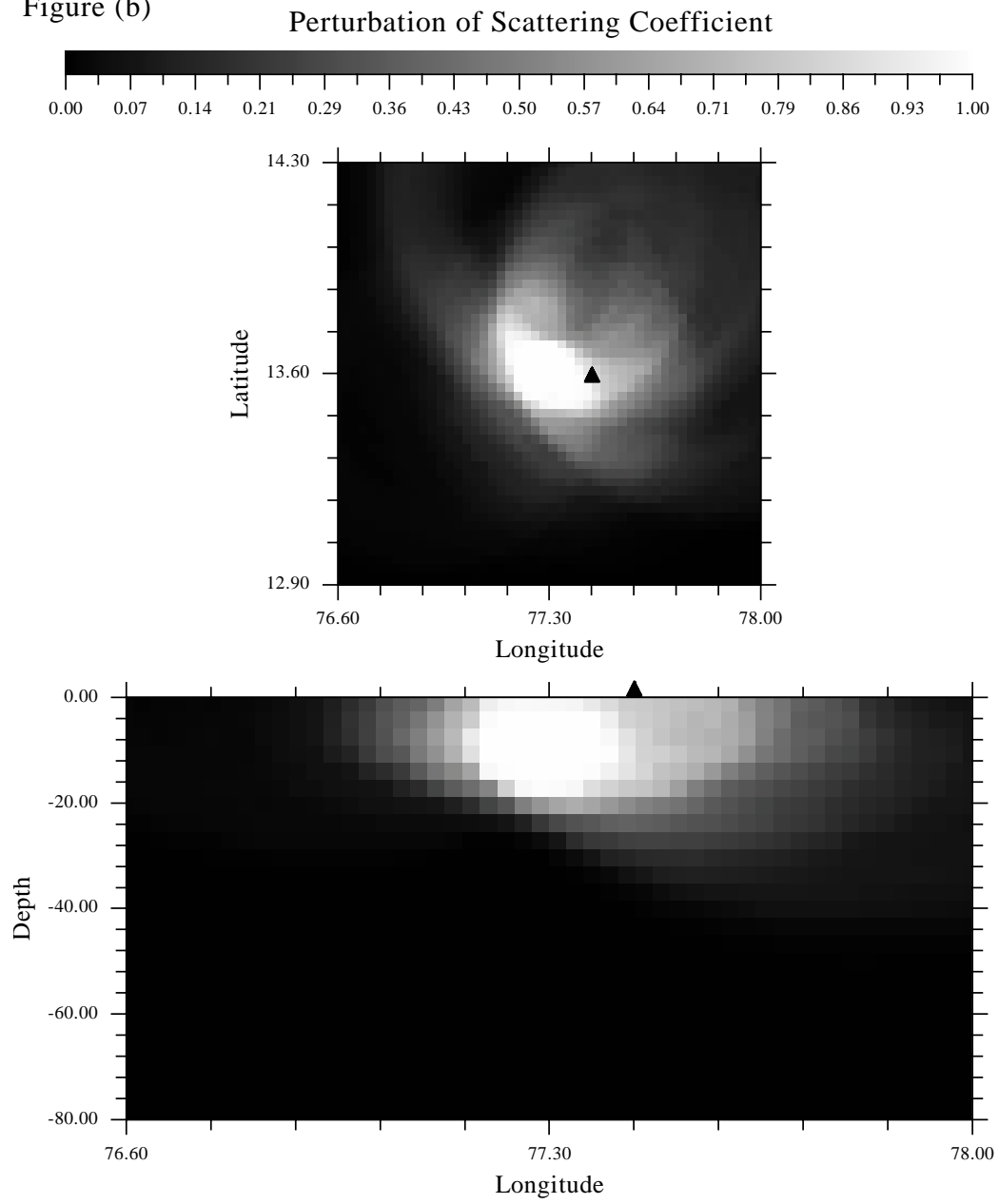


Figure 5-11. (Continued)

Figure (c)

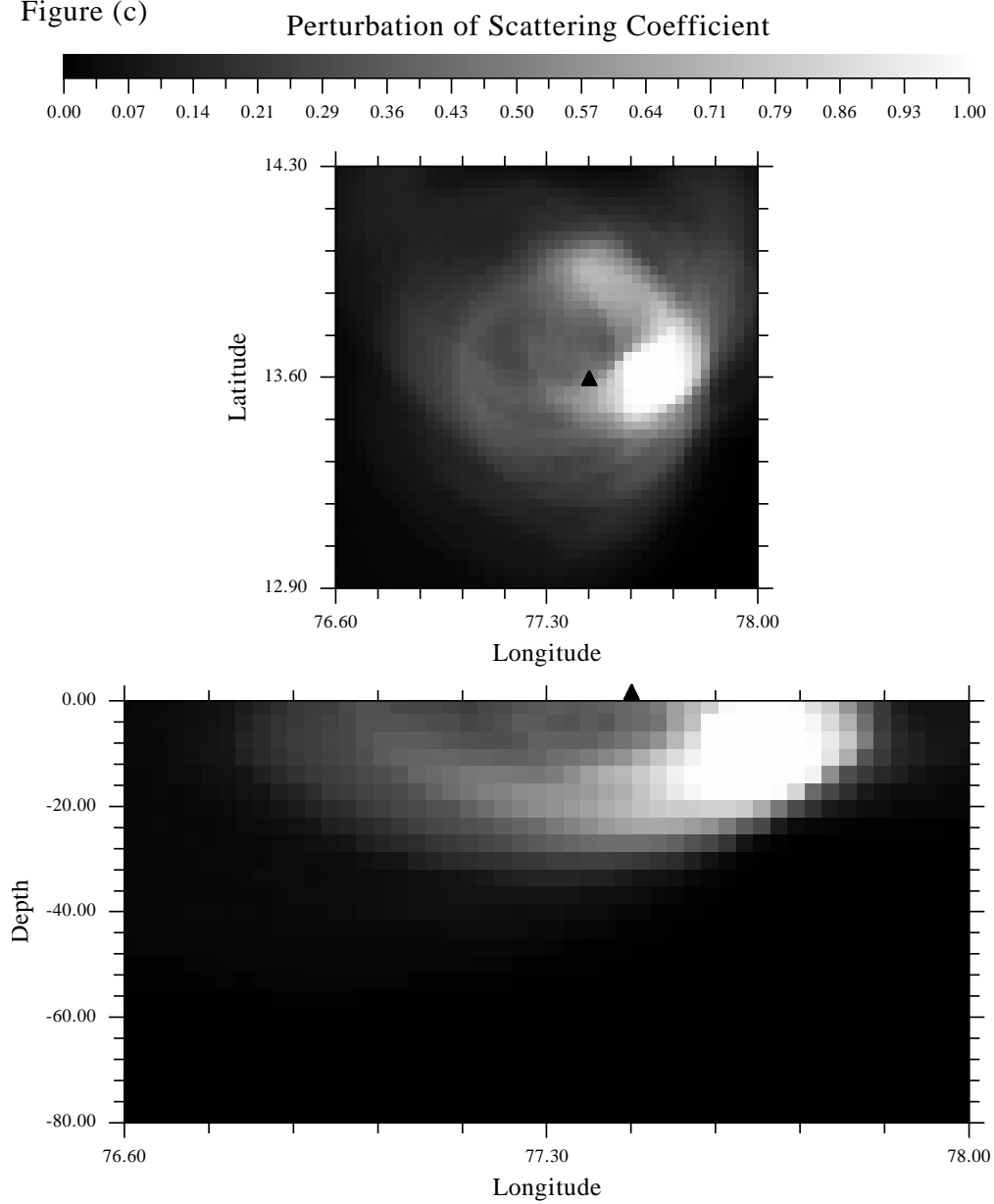


Figure 5-11. (Continued)

5.7 CONCLUSIONS

We estimated the three-dimensional distribution of relative scattering coefficients in the crust in southern India by means of an S-wave coda envelope inversion technique applied to local recordings by the Gauribidanur seismic array. Two different inversion algorithms were used for the first time in this type of seismological research: the Simultaneous Iterative Reconstruction Technique (SIRT) and the Filtered Back-Projection (FBP) method. The results allowed to reach the following conclusions:

- 1) The spatial distribution of the relative scattering coefficients obtained was almost independent of the inversion method used.
- 2) The FBP method is very convenient and appropriate for solving these kinds of problems because it requires about 100 times less computation time than the SIRT algorithm to invert the data.
- 3) The crust of the analyzed region around GBA showed a remarkably uniform distribution of scatterers at more than the 90% of the area, which is in accordance with the conclusions of previous studies in the region using statistical analysis of observed teleseismic traveltime residuals.
- 4) An inhomogeneous structure with size comparable to a wavelength of ~ 1.8 to ~ 3.6 km for 1.5 Hz was detected to the west of GBA from the surface up to a depth of about 24 km just below the array and it coincides with the Closepet granitic intrusion which is the major geological boundary between the eastern and western Dharwar craton.